A phase and space coherent direct imaging method

Songming Hou

Mathematics and Statistics,

Louisiana Tech University,

Ruston LA 71272[a)]

Kai Huang

Department of Mathematics,

Florida International University,

Miami FL 33199[b)]

Knut Solna and Hongkai Zhao

Department of Mathematics,

University of California at Irvine,

Irvine CA 92697.[c)]

(Dated: October 3, 2008)

Abstract

A direct imaging algorithm for point and extended targets are presented. The algorithm is based on a physical factorization of the response matrix of a transducer array. The factorization is used to transform a passive target problem to an active source problem and to extract principal components (tones) in a phase consistent way. The Multi-tone imaging function that can superpose multiple tones (spatial diversity/aperture of the array) and frequencies (bandwidth of the probing signal) based on phase coherence. The method is a direct imaging algorithm which is simple and efficient since no forward solver or iteration is needed. Robustness of the algorithm with respect to noise is demonstrated via numerical examples.

PACS numbers: 43.60.Pt, 43.60.Tj

I. INTRODUCTION

In reflection seismology, ultrasound imaging in medical applications, detection of defects in nondestructive testing, underground mine detection and target detection using radar or a sonar system and so on one seeks to identify the location and shape of some scatterers by sending probing waves and measuring the scattered waves, e.g., using scattering relations. This is in general an ill-posed (non-linear) inverse problem. Imaging the whole medium using a general inverse problem approach may be too complicated and too expensive to be practical in many applications, for instance if the imaging domain is large compared to the wavelength. If the background medium is homogeneous and some simple boundary condition is satisfied at the boundary of the target, the inverse problem can be turned into a geometric problem, that is, the problem of determining the shape of the target from the scattered wave field pattern. Using non-linear optimization approach in this case is still difficult and computationally expensive.

Direct imaging methods, which are not based on non-linear optimization and hence do not require forward solver or iterations, have attracted a lot of attention recently. If the targets are small compared to the array resolution, the location information can be obtained while the geometry information is not resolved. Several matched filter type of algorithms have been developed for imaging or locating point targets, for example the MUltiple SIgnal Classification (MUSIC) algorithm[1–6]. Under the assumption of point targets the response matrix (defined in Section II) has a simple structure. This structure is used in MUSIC and has also been exploited to focus a wave field on selected scatterers using iterated time reversal[7–12]. The iterated time reversal procedure corresponds to the power method for finding the dominant singular vectors for the response matrix. However, with the point target assumption, physical properties and the geometry of the target are neglected. More

[a)]Electronic address: shou@latech.edu
[b)]Electronic address: khuang@fiu.edu
[c)]Electronic address: ksolna,zhao@math.uci.edu

importantly an extended target is not a superposition of point targets. For extended targets the response matrix has a more complicated structure. Recently a few MUSIC type of algorithms[13–16] have been developed to image the location and shape of extended targets. A crucial step is to use resolution and noise level based thresholding to determine how many singular vectors of the response matrix span the signal space.

Although the generalized MUSIC algorithm for a single frequency is capable of imaging different types of targets with efficiency, robustness and accuracy, provided full aperture data is given, for limited aperture the results are typically not very good. Multiple frequencies should be used to complement the lack of spatial aperture.

The MUSIC algorithm is based on the singular value decomposition (SVD) of the response matrix. This decomposition allows for an arbitrary complex phase, therefore, combining different frequencies in a phase coherent way is not direct. In this paper, we propose a multi-tone imaging algorithm that makes use of coherent information in both phase and space. In particular, we take advantage of phase coherence from multiple frequency data to improve both resolution of robustness of the imaging procedure. The crucial points in our multi-tone algorithm are (1) physically based factorization of the response matrix that transforms a passive target detection problem to an active source detection problem, (2) a phase coherent imaging function that can superpose multiple tones and multiple frequencies to take advantage of both spatial diversity (aperture) of the array and/or the bandwidth of the probing signal. The proposed method can be parallelized easily since the evaluation of the imaging function at different grids are independent.

The outline of the paper is as follows. In Section II we describe how to locate point targets using a method that we call the multi-tone algorithm. In Section III, we generalize the method to imaging of extended targets. Numerical experiments are presented in Section IV.

II. RESPONSE MATRIX AND IMAGING POINT TARGETS

Our imaging setup uses an array of transmitters that can send out probing waves into the region of interest and an array of receivers that can record scattered waves. Our measurement data is the response matrix whose elements are the inter-responses between array elements. The arrays can enclose the region of interest (full aperture) or can have partial aperture. For simplicity, we first consider an active array when the array of transmitters and the array of receivers coincide, moreover, time harmonic waves. Assume that there are N transducers, which can function both as a transmitter and as a receiver, and that are located at $\boldsymbol{\xi}_1, \ldots, \boldsymbol{\xi}_N$. The P_{ij} element of the response matrix P is the received signal at transducer j for a probing pulse sent out from transducer i. Assume that there are M point targets located at $\boldsymbol{x}_1, \ldots, \boldsymbol{x}_M$ with reflectivity $\tau_1, \ldots, \tau_M$. The response matrix in the Born approximation has the following simple structure using spatial reciprocity

$$\begin{aligned} P_{ij} &= \sum_{m=1}^{M} \tau_m G^0(\boldsymbol{x}_m, \boldsymbol{\xi}_i) G^0(\boldsymbol{\xi}_j, \boldsymbol{x}_m) \\ &= \sum_{m=1}^{M} \tau_m G^0(\boldsymbol{\xi}_i, \boldsymbol{x}_m) G^0(\boldsymbol{\xi}_j, \boldsymbol{x}_m), \end{aligned}$$

where $G^0(\boldsymbol{x}, \boldsymbol{y})$ is the free space Greens function and we suppress the dependence on frequency. In matrix form we have

$$P = \sum_{m=1}^{M} \tau_m \mathbf{g}_m \mathbf{g}_m^T,$$

where

$$\mathbf{g}_m = \left[G^0(\boldsymbol{\xi}_1, \boldsymbol{x}_m), G^0(\boldsymbol{\xi}_2, \boldsymbol{x}_m), \ldots, G^0(\boldsymbol{\xi}_N, \boldsymbol{x}_m) \right]^T,$$

$m = 1, 2, \ldots, M$, are called illumination vectors, each of which corresponds to the received signals at the array for a point source at $\boldsymbol{x}_m$. For an active array, the response matrix is square and symmetric with rank M in general. If the targets are well resolved by the transducer array, i.e., the separation distance between the targets is larger than the resolution of the array, we have that the point spread function

$$\Gamma(\boldsymbol{x}_m, \boldsymbol{x}_{m'}) = \overline{\mathbf{g}}_m^T \mathbf{g}_{m'} \approx 0 \text{ if } m \neq m',$$

which means the wave field corresponding to the time reversal of a point source at one target is almost zero at all other targets. Hence $\hat{\mathbf{g}}_m = \frac{\mathbf{g}_m}{\|\mathbf{g}_m\|}$ and its complex conjugate $\overline{\hat{\mathbf{g}}}_m$ can be regarded as the left and right singular vector for the response matrix P. In general this one to one correspondence does not exit. However one can show that $\mathbf{g}_m, m = 1, 2, \ldots, M$ still span the signal space of P even if multiple scattering among point targets is present based on the Foldy-Lax formulation[2].

Remark: Here we assume the simplest model for point scatters. In general, a point scatterer may induce both monopole and dipole for the scattered field. For example the scattered field for an acoustic point scatterer is the sum of monopole (by contrast in compressibility) and dipole (by contrast in density)[17,18]. Our formulation and imaging function only uses the monopole component which works for hard scatterers. We should be able to modify our imaging function to take into account diploe which will be discussed in our future work.

To motivate our imaging algorithm consider first the case with a point source at the m'th scatterer location, the vector of observations at the transducer array is then

$$\mathbf{g}(\boldsymbol{x}_m) = \left[G^0(\boldsymbol{\xi}_1, \boldsymbol{x}_m), G^0(\boldsymbol{\xi}_2, \boldsymbol{x}_m), \ldots, G^0(\boldsymbol{\xi}_N, \boldsymbol{x}_m)\right]^T.$$

Phase conjugation at the mirror and back-propagation to the imaging domain corresponds to forming the imaging function: $I_m(\boldsymbol{x}) = \mathbf{g}(\boldsymbol{x}_m)^H \mathbf{g}(\boldsymbol{x})$, where $\boldsymbol{x}$ is a search point in the domain and the superscript H denotes the transpose and complex conjugate. Note that physical *time-reversal* corresponds to phase conjugation in frequency domain and then back-transformation to time domain. In the inverse problem setting, although $\boldsymbol{x}_m$ is unknown, an estimate of $\hat{\mathbf{g}}(\boldsymbol{x}_\mathbf{m})$ can be obtained (up to a constant phase) via the singular value decomposition of the response matrix. The imaging function will peak at the source location $\boldsymbol{x}_m$ due to phase coherence; $I_m(\boldsymbol{x}_m) = \|\mathbf{g}(\boldsymbol{x}_m)\|^2$. In particular if we use normalized $\hat{\mathbf{g}}(\boldsymbol{x})$ and $\hat{\mathbf{g}}(\boldsymbol{x}_m)$ in the above imaging function, it is an optimal matched filter[19**?**,20]. Classic Rayleigh resolution theory gives that $I_m(\boldsymbol{x})$ will be supported in the neighborhood of the source-point $\boldsymbol{x}_m$ with a lateral resolution of order $\lambda L/a$. Here $\lambda = c_0/\omega$ is the wavelength, L the distance from the array to the source and a the aperture of the array and c_0 denotes

the speed of propagation.

We compute the Singular Value Decomposition (SVD) of the response matrix to extract dominant singular vectors (tones). This matrix factorization corresponds to turning passive targets into imaging sources for the scattered wave. However, the SVD of a matrix is unique up to a complex phase, e.g, if the following is a SVD of P

$$P = \sum_m \sigma_m \mathbf{u}_m \mathbf{v}_m^H,$$

where $\mathbf{u}_m(\mathbf{v}_m)$ are the unit left (right) singular vectors and σ_m are the singular values of P, then $e^{i\theta_m}\mathbf{u}_m(e^{i\theta_m}\mathbf{v}_m)$ are also left (right) singular vectors for arbitrary $\theta_m, m = 1, 2, \ldots$. To overcome the arbitrary phase in the SVD, we propose the following modified imaging function for each pair of left and right singular vectors $\mathbf{u}_m$ and $\mathbf{v}_m$, which we call a tone of the response matrix,

$$I_m(\boldsymbol{x}) = [\hat{\mathbf{g}}^H(\boldsymbol{x})\mathbf{u}_m][\hat{\mathbf{g}}^H(\boldsymbol{x})\overline{\mathbf{v}}_m].$$

First, this imaging function removes the phase ambiguity of the SVD of the response matrix. Second, for well resolved point targets,

$$I_m(\boldsymbol{x}) = [\hat{\mathbf{g}}^H(\boldsymbol{x})\hat{\mathbf{g}}(\boldsymbol{x}_m)]^2.$$

Note that by "squaring" in this way, instead of using norm square, we maintain the phase information, e.g., the phase information is just linearly doubled. Next, we superpose the dominant tones for the different frequencies to obtain the general form of the multi-tone imaging function:

$$I^M(\boldsymbol{x}) = \sum_\omega \alpha(\omega) \sum_{m=1}^{M^\omega} [\hat{\mathbf{g}}^H(\boldsymbol{x};\omega)\mathbf{u}_m^\omega][\hat{\mathbf{g}}^H(\boldsymbol{x};\omega)\overline{\mathbf{v}}_m^\omega]. \tag{1}$$

We remark that for an active array with the transmitters and receivers coinciding, the response matrix P is complex symmetric, and can be factorized as $P = U\Sigma U^T$. The imaging function then becomes

$$I^M(\boldsymbol{x}) = \sum_\omega \alpha(\omega) \sum_{m=1}^{M^\omega} [\hat{\mathbf{g}}^H(\boldsymbol{x};\omega)\mathbf{u}_m^\omega]^2. \tag{2}$$

In the general case when the transmitters and receivers do not coincide, e.g., there are s transmitters located at $\boldsymbol{\xi}_1, \ldots, \boldsymbol{\xi}_s$ and there are r receivers located at $\boldsymbol{\eta}_1, \ldots, \boldsymbol{\eta}_r$, the response matrix is of dimension $s \times r$. The $ij'th$ element P_{ij} then records the response at j-th receiver for a signal sent out from i-th transmitter. Define the illumination vector with respect to the receiver array and transmitter array respectively as

$$\mathbf{g}_r(\boldsymbol{x}) = [G^0(\boldsymbol{\eta}_1, \boldsymbol{x}), G^0(\boldsymbol{\eta}_2, \boldsymbol{x}), \ldots, G^0(\boldsymbol{\eta}_r, \boldsymbol{x})]^T,$$

and

$$\mathbf{g}_s(\boldsymbol{x}) = [G^0(\boldsymbol{\xi}_1, \boldsymbol{x}), G^0(\boldsymbol{\xi}_2, \boldsymbol{x}), \ldots, G^0(\boldsymbol{\xi}_s, \boldsymbol{x})]^T.$$

The response matrix in the Born approximation has the following form in the case of M point targets located at $\boldsymbol{x}_1, \ldots, \boldsymbol{x}_M$ with reflectivity $\tau_1, \ldots, \tau_M$

$$P = \sum_{m=1}^{M} \tau_m \mathbf{g}_s(\boldsymbol{x}_m) \mathbf{g}_r^T(\boldsymbol{x}_m).$$

Thus, the column and row space of P is spanned by $\mathbf{g}_s(\boldsymbol{x}_m)$ and $\mathbf{g}_r^T(\boldsymbol{x}_m)$ respectively. Accordingly the multi-tone imaging function is constructed as

$$I^M(\boldsymbol{x}) = \sum_{\omega} \alpha(\omega) \sum_{m=1}^{M^\omega} [\hat{\mathbf{g}}_s^H(\boldsymbol{x}; \omega) \mathbf{u}_m^\omega][\hat{\mathbf{g}}_r^H(\boldsymbol{x}; \omega) \overline{\mathbf{v}}_m^\omega]. \tag{3}$$

Here $\hat{\mathbf{g}}$ denotes the normalized illumination vector.

The frequency weight function $\alpha(\omega)$ can in principle be chosen to reflect the signal to noise ratio of different frequencies. However, here we will not discuss this issue and use a uniform weighting. Note second that M^ω is the number of significant tones which may vary with frequency. If there are M point targets that are well resolved by all the frequencies used, then $M^\omega = M$. In general, e.g., for extended targets, M^ω may be proportional to the resolution of frequency ω[13,21]. In particular when there is strong noise present, e.g., low signal to noise ratio (SNR), M^ω is an important thresholding (regularization) parameter[13]. An important strength of the multi-tone algorithm is that it is quite robust with respect to the choice of M^ω. In particular when the noise level is low, we can choose it to coincide with the smaller dimension of the response matrix. This is not the case for for instance the

MUSIC algorithm, described below, whose imaging result depends more sensitively on the thresholding.

We summarize by stating that two important features of the multi-tone imaging algorithm are:

1. The SVD factorization of the response matrix turns a passive target detection problem into an active source detection problem. The principal component (tone) decomposition of the response matrix takes the full array into account simultaneously and extracts dominant information or "tones" via the singular value decomposition, giving a robust imaging scheme.

2. The imaging function exploit coherent phase information via superposition of complex tones.

Next, we compare our multi-tone imaging algorithm with two other popular imaging algorithms. For simplicity we discuss the active array case.

1. MUSIC. The MUSIC imaging function[1,6] is based on the projection to the signal space spanned by dominant singular vectors, which is equivalent to the following quantity:

$$\sum_{m=1}^{M} |\hat{\mathbf{g}}^H(\boldsymbol{x})\mathbf{u}_m|^2$$

where M is the dimension of the signal space that is determined according to the resolution and/or the signal to noise ratio (SNR) analysis[13,21]. However, phase information is lost after projection and hence it is difficult to superpose multiple frequencies based on phase coherence. Thus, travel time information is not effectively utilized in this implementation of the MUSIC imaging functional.

2. Kirchhoff migration. The Kirchhoff migration is a time domain method which exploit travel time information between pairs of transducers. After Fourier transform it can be approximated in frequency domain[22] by the following:

$$\tilde{\mathbf{g}}^H(\boldsymbol{x})P\overline{\tilde{\mathbf{g}}}(\boldsymbol{x}) = \tilde{\mathbf{g}}^H(\boldsymbol{x}) \left[\sum_{m=1}^{N} \sigma_m \mathbf{u}_m \mathbf{v}_m^H\right] \overline{\tilde{\mathbf{g}}(\boldsymbol{x})},$$

where $\tilde{\mathbf{g}}(\boldsymbol{x})$ is the Green's function without the spatial decaying factor $(1/\|\boldsymbol{x}\|)$ and N is the number of transducers. The above formula is similar to (1) for each frequency except the following two main differences: (1) our imaging function does not contain the weighting by the singular values, (2) our imaging function introduces a thresholding/regularization based on resolution and/or SNR. These two differences mean that the multi-tone imaging algorithm only separates signal space from noise space and treats all dominant signals, i.e, dominant singular vectors, equally. The motivation comes from the following observations: a point target partially blocked by other targets will contribute a singular vector with smaller singular values. So our multi-tone imaging function will increase the visibility of partially blocked targets compared to Kirchhoff migration as shown in Figure 2 and Figure 3 in Section IV.A. Also an extended target is not a superposition of point targets. For example it is illustrated in[13] that each singular vector does not correspond to a point on the boundary of an extended target. The geometry of the boundary is embedded in the signal space spanned by the dominant singular vectors collectively. Hence the multi-tone imaging function will serve to give an uniform illumination of the visible parts of the boundary.

In summary our multi-tone imaging algorithm takes advantages of both approaches in a natural way. Like MUSIC, our algorithm is based on the SVD of the response matrix and a resolution and/or SNR based thresholding, to extract principal components (tones) from the full array information. The principal components are used collectively and in an uniform weighting situation. This is particularly important for imaging extended targets. The response matrix for an extended target can have many principal components[14,18,23–27]. The collection of all these principal components contains information about the extended target. On the other hand, instead of using a projection operator as in MUSIC, we use a propagation operator as in the Kirchhoff method which maintains coherent phase information and allows linear superposition of different tones (components) and multiple frequencies. Only at locations with strong scattering are phases of different tones and different frequencies in our imaging function coherent. Like in the Kirchhoff method travel time information is thus

utilized in our imaging function. Our approach is based on gaining robustness via using the singular value decomposition of the response matrix to extract coherent information and is extremely simple to implement. We remark that other recent approaches like the CINT method[22] aim at extracting information via carefully screened cross correlation computations of the observations. This approach has been shown to work quite well in a strongly heterogeneous environment but is less direct in its implementation.

III. EXTENDED TARGETS

A. Dirichlet Boundary Condition

We consider the situation with an extended target. First, let us assume a Dirichlet boundary condition for the target, i.e., a sound soft target. Let Ω denote the target and Ω^c the exterior of the target. Let $G_\Omega(\boldsymbol{x}, \boldsymbol{y})$ be the associated Green's function that solves

$$\begin{cases} \Delta G_\Omega(\boldsymbol{x}) + k^2 G_\Omega(\boldsymbol{x}) = \delta(\boldsymbol{x} - \boldsymbol{y}) & \boldsymbol{x}, \boldsymbol{y} \in \Omega^c \subset R^m \\ G_\Omega(\boldsymbol{x}, \boldsymbol{y}) = 0 & \boldsymbol{x} \in \partial\Omega, \end{cases}$$

and a far field radiation boundary condition. The scattered field at transducer $\boldsymbol{\xi}_j$ corresponding to a point source at $\boldsymbol{\xi}_i$ follows from Greens formula and is

$$P_{ij} = \int_{\partial\Omega} G^0(\boldsymbol{\xi}_i, \boldsymbol{y}) \frac{\partial G_\Omega(\boldsymbol{\xi}_j, \boldsymbol{y})}{\partial \nu} d\boldsymbol{y}\,,$$

where G^0 is the free space Green's function. A physical interpretation is that the source of the scattered wave field is a weighted superposition of monopoles at the boundary. The response matrix can be written

$$P = \int_{\partial\Omega} \mathbf{g}(\boldsymbol{y}) \left[\frac{\partial \mathbf{g}_\Omega(\boldsymbol{y})}{\partial \nu} \right]^T d\boldsymbol{y}\,, \tag{4}$$

where $\mathbf{g}(\boldsymbol{y})$ is the illumination vector for the homogeneous background, which is known, and $\mathbf{g}_\Omega(\boldsymbol{y})$ is the illumination vector

$$g_\Omega(\boldsymbol{y}) = [G_\Omega(\boldsymbol{\xi}_1, \boldsymbol{y}), \ldots, G_\Omega(\boldsymbol{\xi}_N, \boldsymbol{y})]^T,$$

which is unknown.

The equation (4) gives a factorization of the response matrix that separates the known and unknown components. Thus, the response matrix is superposed from illumination vector $\mathbf{g}(\boldsymbol{y})$, where $\boldsymbol{y}$ belongs to the illuminated parts of the boundary, e.g., where $\frac{\partial \mathbf{g}_\Omega(\boldsymbol{y})}{\partial \nu}$ is not small. Therefore we apply SVD to the response matrix to extract the singular vectors $\mathbf{u}_m(\mathbf{v}_m)$ and then use the imaging functions (2) for symmetric active array and (3) if the transmitter array and receiver array are different. This imaging function will peak at the well illuminated parts of the boundary. Physically, the peak can be explained by the fact that the boundary becomes as the source for the scattered field and iterated time reversal, i.e., power method for finding singular vectors, will focus on the boundary. The thresholding strategy for extended targets introduced in[13] can be used to determine the thresholding parameter by an optimal cutoff.

We remark that the unknown weight function (illumination strength) for the monopoles at the target boundary, $\frac{\partial \mathbf{g}_\Omega(\boldsymbol{y})}{\partial \nu}$, is not uniform in general due to geometry of the target, such as singularities and concavity of the boundary, and/or the array configuration, such as illumination angles and partial aperture. Locations on the boundary with stronger wave field, i.e, better illuminated by the source, have more weights. These factors will be reflected by the magnitude of singular values for different singular vectors. In our multi-tone algorithm each principal component will be given an equal weight as long as its corresponding singular value is above the noise threshold. That is why our imaging function give a fairly uniform intensity on the well illuminated boundary. This is an important aspect of our approach: by taking out the scaling of the tones by the singular values we focus on the geometrical aspects of the extended scatterer and compensates for differences in relative illumination strength. Thus differential parts of the boundary is imaged with a similar fidelity.

B. Neumann Boundary Condition

For a sound-hard target, with a Neumann boundary condition for the extended target the response matrix has the form

$$P = -\int_{\partial\Omega} \left[\frac{\partial \mathbf{g}(\boldsymbol{y})}{\partial \nu}\right] \mathbf{g}_{\Omega}^{T}(\boldsymbol{y}) d\boldsymbol{y}\,.$$

In other words, the source of the scattered wave field is a (unknown) weighted superposition of dipoles $\frac{\partial \mathbf{g}(\boldsymbol{y})}{\partial \nu}$ at the boundary. Therefore, the normal direction is part of the unknown in the imaging function. As is done in[13] we will incorporate a direction search in our imaging function, e.g., among a fixed collection of discretized directions, $\mu_j, j = 1, 2, \ldots$, we maximize the imaging function among these directions at a searching point $\boldsymbol{x}$. Our Multi-tone imaging function is then in the general case:

$$I^M(\boldsymbol{x}) = \max_j \left| \sum_{\omega} \alpha(\omega) \sum_{m=1}^{M^\omega} \left[\frac{\partial \hat{\mathbf{g}}_s^H(\boldsymbol{x};\omega)}{\partial \nu_j} \mathbf{u}_m^\omega\right] \left[\frac{\partial \hat{\mathbf{g}}_r^H(\boldsymbol{x};\omega)}{\partial \nu_j} \overline{\mathbf{v}}_m^\omega\right] \right|.$$

C. Limited or Synthetic Aperture

For single frequency and full aperture the MUSIC algorithm typically works better than Multi-tone. However, for limited aperture or synthetic aperture with multiple frequency data MUSIC may fail while Multi-tone can work well. We demonstrate below that the multi-tone algorithm works well also in a case with limited or synthetic aperture.

D. Far field data

In the previous sections the response matrix is defined in terms of near field data, with the sources and receivers in near field. In some applications, the measurement data is far field data, that is, the incident field is essentially a plane wave and the far field pattern of the scattered field is recorded.

We now discuss briefly the case for far field data. For Dirichlet boundary condition, the element of the response matrix P_{ij} corresponds to the far field pattern of the scattered field

in the jth direction due an incident wave coming from the ith direction:

$$P_{ij} = u_\infty(\hat{\boldsymbol{\theta}}_j; \hat{\boldsymbol{\theta}}_i) = \beta \int_{\partial\Omega} \frac{\partial u}{\partial \nu}(\boldsymbol{y}; \hat{\boldsymbol{\theta}}_i) e^{-ik\hat{\boldsymbol{\theta}}_j \cdot \boldsymbol{y}}\, d\boldsymbol{y},$$

where the total field u is due to incident plane wave coming from the direction $\hat{\boldsymbol{\theta}}_i$, where $\beta = -\frac{1}{4\pi}$ for three dimensions and $\beta = -\frac{e^{i\pi/4}}{\sqrt{8\pi|k|}}$ for two dimensions.

In matrix form

$$P = \beta \int_{\partial\Omega} \frac{\partial \vec{u}}{\partial \nu} \hat{\mathbf{g}}^H(\boldsymbol{y}) d\boldsymbol{y}, \tag{5}$$

where

$$\hat{\mathbf{g}}(\boldsymbol{y}) = [e^{ik\hat{\boldsymbol{\theta}}_1 \cdot \boldsymbol{y}}, \ldots, e^{ik\hat{\boldsymbol{\theta}}_n \cdot \boldsymbol{y}}]^T,$$

and $\vec{u}$ is the vector of total fields corresponding to the incident plane waves from $\hat{\boldsymbol{\theta}}_1, \ldots, \hat{\boldsymbol{\theta}}_n$. Equation (5) gives a physical factorization of the scattered field into known and unknown parts. The far field pattern is a superposition of the far field patterns of point sources located on the boundary of the target, however, we do not know the weight function which depends on the total field. In other words, the scattering at the target boundary acts as "sources" for the scattered field. In this far field setup, it is natural to use $\hat{\mathbf{g}}(\boldsymbol{y})$ as the illumination vector as discussed in[14]. The signal space of the response matrix should be well approximated by the span of the illumination vectors $\hat{\mathbf{g}}(\boldsymbol{y})$ with $\boldsymbol{y}$ on the well-illuminated part of the boundary of the targets. Hence, we only need to change the form of illumination vectors in the Multi-tone imaging function. Neumann type of boundary conditions can also be dealt in a similar fashion as in the case with near field data. See[14] for more details.

IV. NUMERICAL EXPERIMENTS

A. Point targets

First we show a few examples for point targets, targets that are small compared to the resolution of the array. The examples are 2D experiments and simulations.

In the first numerical test, there are three targets with a range of $30 - 40\lambda$ (central wavelength). The linear active array is located at the left side and is composed of 21

transducers that are half wavelength apart, i.e., the aperture is 10λ. The three targets are of size 0.5λ each. We tested this setup in both homogeneous and random media. The weakly heterogeneous medium has a 5% standard deviation and the correlation length is $O(\lambda)$. Finite difference method is used to solve the Helmholtz equation with perfectly matched layer (PML) technique[28] for 21 frequencies that are equally distributed between 0.9λ and 1.1λ with equal weight. The size of grid in numerical scheme is $\lambda/10$ in the 2D rectangle domain. The star shows the true location of targets.

Figure 1 shows the singular value decomposition (SVD) pattern for a fixed frequency (1.1λ) for these two cases. In the homogeneous medium, there are only three dominant singular values. However, it is clear that the corresponding three singular vectors do not have a one to one correspondence to the illumination vector of the three targets due to multiple scattering among the targets.

The numerical data used for imaging targets in heterogeneous medium is the scattered wavefield by the target and the background heterogeneous medium, i.e., the the difference of the two wavefields corresponding to the medium with targets and the homogeneous medium respectively. The goal is to image dominant scatterers/targets without imaging or knowing the details of the background medium, which is very desirable in many practical applications. The situation is also more difficult than using the difference data, i.e., measuring the difference of the two wavefields corresponding to the medium with targets and the same medium without targets respectively. Figure 2 and Figure 3 shows the imaging results using multi-tone imaging algorithm using different number of frequencies and different number of leading singular vectors. It shows clearly that:

- Superposition of coherent phases from multiple frequencies improves range resolution.
- Using the leading three singular vectors (the best SNR thresholding) produces the best results, However, the imaging result is not very sensitive to thresholding.
- The partially blocked target has a better visibility compared to the Kirchhoff migration for the reason discussed in Section II.

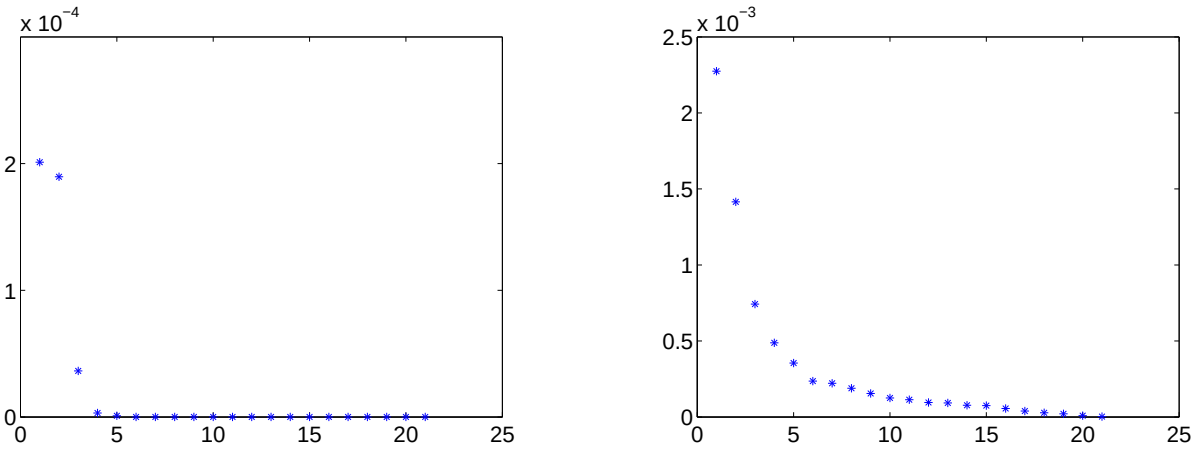

(a) homogeneous medium (b) random medium

FIG. 1. SVD pattern of the response matrix.

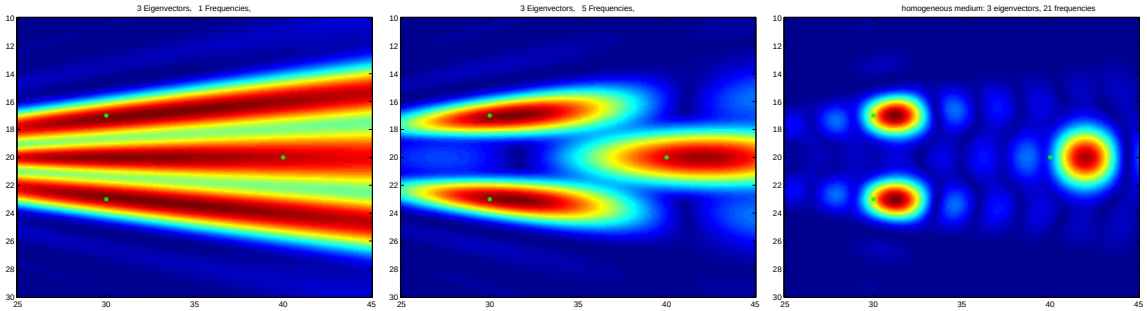

(a) (b) (c)

FIG. 2. Imaging point targets in homogeneous medium. Multi-tone algorithm using 3 leading singular vectors and (a) 1 frequency, (b) 5 frequencies, and (c) 21 frequencies.

As shown in Figure 1, the SVD pattern is more complicated in random medium due to multi-pathing. Figure 4 shows the imaging results using the multi-tone imaging algorithm, which demonstrates the following:

- The location information of three point targets is not included in the first three singular vectors.
- Involving more singular vectors, even without thresholding, works well since only strong scattering at targets are superposed coherently (in phase) across different fre-

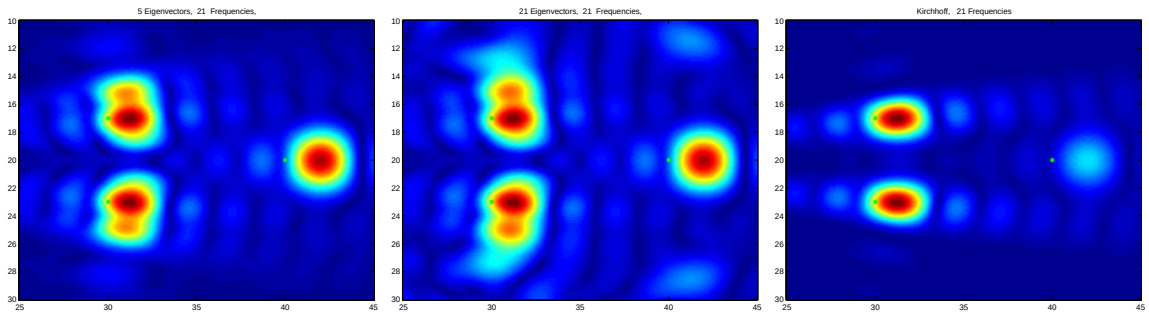

(d) (e) (f)

FIG. 3. Imaging point targets in homogeneous medium. Multi-tone algorithm using 21 frequencies and (d) 5 leading singular vectors, (e) 21 singular vectors. (f) Kirchhoff algorithm using 21 frequencies.

quencies.

- Again the partially blocked target has a better visibility compared to the Kirchhoff migration.

Finally we test our algorithms on real experimental data. The data was kindly provided by Daniel D. Stancil and his group at Carnegie Mellon University. In their experimental setup, transmit array A and receive array B are used as shown in Figure 5. The locations of transmitters and receivers are different. The measurements were taken at 201 frequency points ranging from $4GHz$ to $6GHz$. An absorbing wall is located behind the test scenario.

The Figures 6 shows imaging using data with different number of targets. The stars in each figure are the true locations of targets.

B. Extended targets

In this section we test our multi-tone imaging algorithm on extended targets with full aperture, limited aperture and synthetic aperture using near and far field data. All near field data are simulated by solving the Helmholtz equation using finite difference method with PML[28] boundary condition. Since the forward solver is not required to be very accurate,

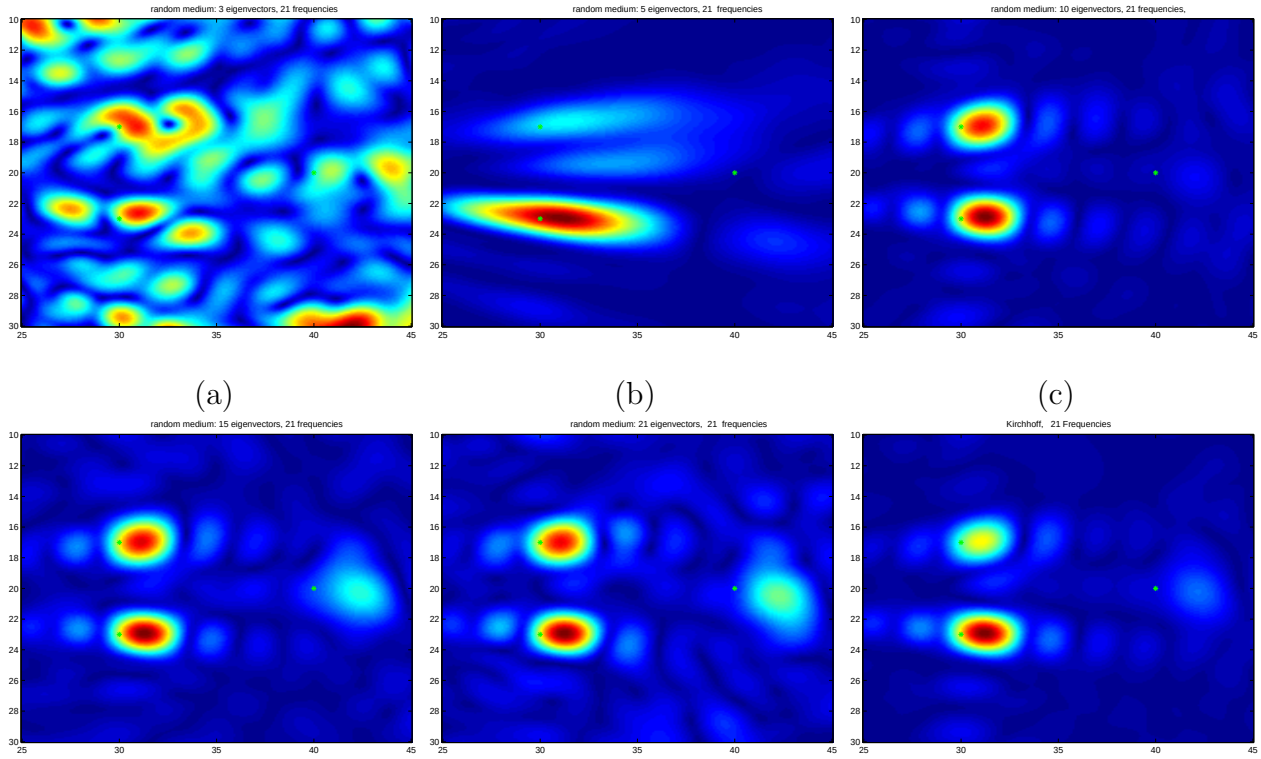

FIG. 4. Imaging point targets in random medium. Multi-tone algorithm using 21 frequencies and (a) 3, (b) 5, (c) 10, (d) 15, and (e) 21 singular vectors, (f) Kirchhoff algorithm using 21 frequencies.

we did not implement special treatment on the target boundary, i.e., the standard stencil is used. Far field data is generated using a boundary integral method[14,29]. The simulations are in 2D.

We give two examples with full or limited aperture near field data, two examples with synthetic aperture near field data, one example with full aperture far field data, one example where sources and receivers do not coincide, finally, one example with limited aperture far field data. For all near field experiments, the transducers are about $200h$ (200 grid cells) away from the target and the forward data is again generated using a finite difference method with the perfectly matched layer (PML) technique[28]. The multiplicative noise is modeled by: $P_{noisy}(i,j) = real(P(i,j)) \cdot a + imag(P(i,j)) \cdot b$, where a, b are uniformly distributed in

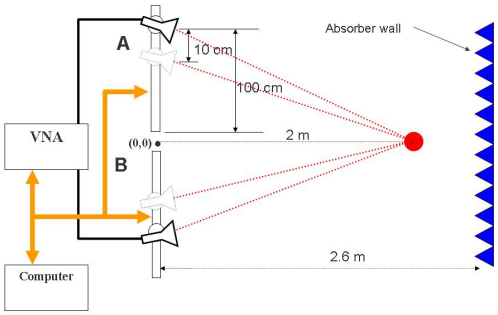

FIG. 5. CMU experiment setup.

$[1-c, 1+c]$, where c is 10%. The random medium or *clutter* is modeled as follows: The index of refraction $n(x)$ is a Gaussian with mean one and standard deviation 10% and the correlation length is $10h$, which is comparable but less than the wave length.

Figure IV.B shows imaging of a single extended target in a homogeneous medium. The full circular active array has 80 transducers surrounding the target. When a single frequency is used the corresponding wavelength is $\lambda = 16h$. When 3 frequencies are used, they correspond to wavelengths, $\lambda = 16h, 24h, 32h$. The target is about $200h$ away from the array and its size is about $80 - 100h$. In this test, no thresholding is used in the multi-tone imaging function. It is clear that phases across different frequencies are superposed coherently at the boundary only, where strong scattering happens. Figure 8 shows imaging of the same target with limited aperture data. Only half of the circular array from the bottom is used.

Figure 9 shows the imaging of a sound-hard (Neumann boundary condition) target with full aperture circular array (80 transducers). The array is about $200h$ from the center of the target. Six equally spaced frequencies are used, with lowest frequency $\lambda = 32h$ and highest frequency $\lambda = 16h$.

We next test with synthetic aperture. We use the following implementation of synthetic aperture. Let P be a 80-by-80 response matrix corresponding to an active circular array with full aperture (as above), and $P_n = Q(n : n + 19, n : n + 19)$, where $n = 1, 11, 21, ...61$, then the P_n's are the 20-by-20 response matrices with limited aperture and a partial overlap. We use P_n at the same 6 frequencies as above.

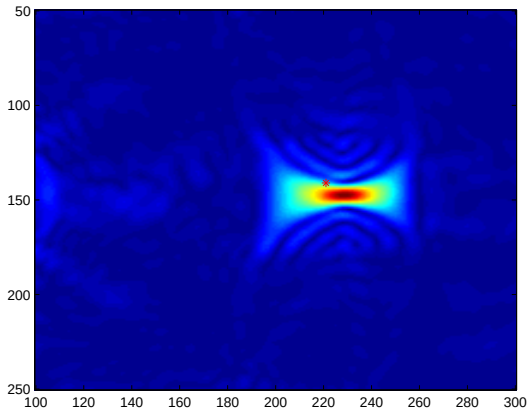

(a) 1 Target

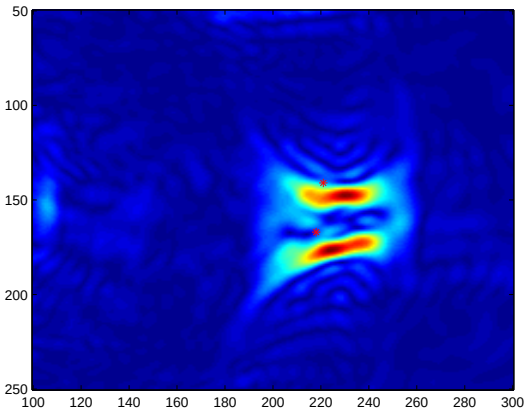

(b) 2 Targets

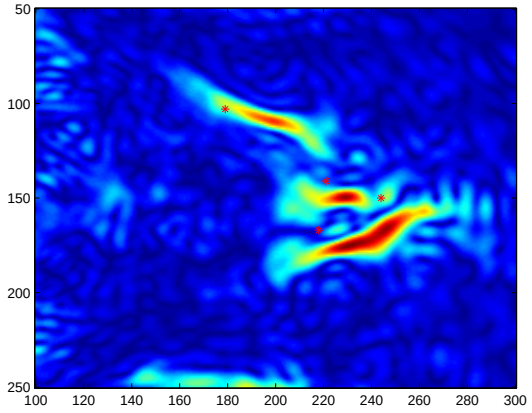

(c) 4 Targets

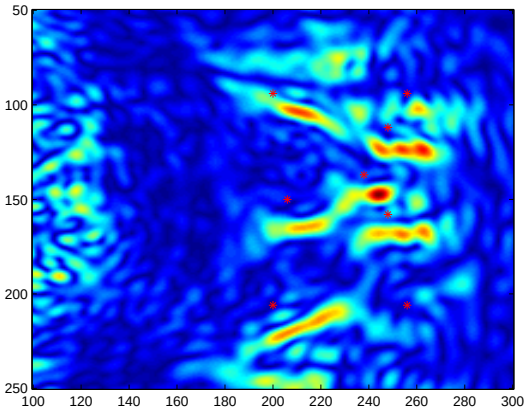

(d) 8 Targets

FIG. 6. CMU experiment data Imaging. (a) 1 Target (b) 2 Targets (c) 4 Targets and (d) 8 Targets.

Figure 10 shows the multi-tone imaging function with synthetic aperture data for a sound-soft (Dirichlet boundary condition) object. The top one is the result for homogeneous medium with clean simulated data. For the middle one, 10% multiplicative noise is added to the data. The bottom one shows imaging in a random medium with 10% standard deviation. The correlation length is about a wavelength.

In contrast, the MUSIC algorithm does not provide a good imaging function for limited/synthetic aperture data. Figure 11 shows the result using the MUSIC algorithm with

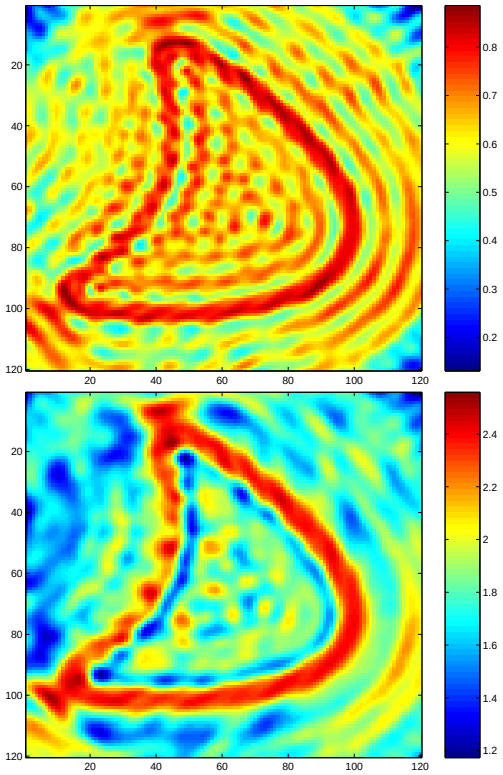

FIG. 7. Multi-tone algorithm using full aperture data with one frequency (top) and three frequencies (bottom).

synthetic aperture data. The kite shape is not clear.

Finally we test the multi-tone imaging algorithm using far field data. The only change made is in the form of the illumination vector, i.e., using the far field pattern of the Greens function. Figure 12 shows the multi-tone imaging function for far field data with clean simulated data (left), and with 100% multiplicative noise added to the simulated data (right). Three wave numbers are used, $k = 5, 6, 7$, so that the target sizes are on the scale of the wavelength. The forward data is here generated using the boundary integral method. In this case 32 plane incident waves are used and the far field data is collected at the same 32 directions.

We remark that the thresholding strategy discussed in[13] is used for all the above examples of extended targets except the first one. In principle, with thresholding only the first few dominant singular vectors are used in the multi-tone imaging function. This is known to

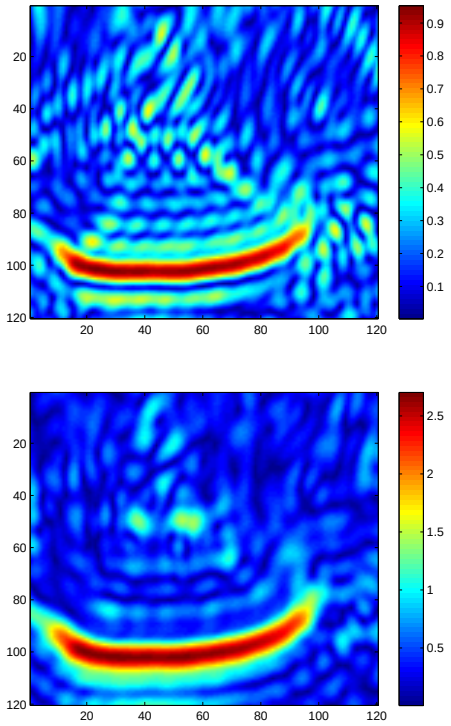

FIG. 8. Multi-tone algorithm using limited aperture data(half of the circular array from the bottom) with one frequency (top) and three frequencies (bottom).

be robust as long as the leading singular values are well separated from the remainder. However, in our tests the results are not very sensitive to the thresholding, which means that the multi-tone imaging function is already quite robust and is easier to use in practice. Thus we also expect that our imaging results are robust with respect to numerical errors and artifacts by our numerical scheme that generate the data.

In the last set of tests, we show imaging with arrays that have transmitters different from receivers, or plane wave incident angles different from far field data angles. Figure 13 shows the multi-tone imaging function using wave numbers $k = 5, 6, 7$ for far field data with plane wave incident from the right (16 directions) and far field pattern recorded on the left (16 directions). Dirichlet boundary condition is used.

Again, for limited aperture only part of the boundary that is well illuminated is seen in the imaging function. Figure 14 shows the multi-tone imaging function using wave numbers

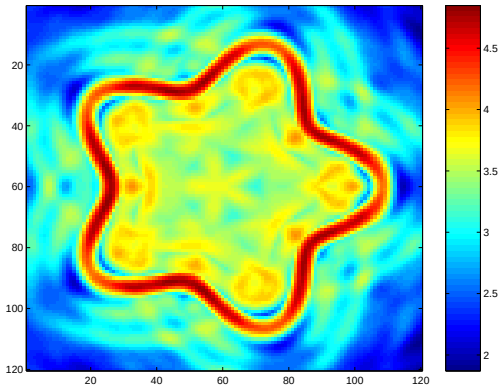

FIG. 9. Imaging of extended target with Neumann boundary condition and full aperture using the multi-tone algorithm with 6 frequencies

$k = 5, 6, 7$ for far field data with limited aperture, that is, only plane waves in a 180 degree angle are used (16 directions) and the far field data within the same angle are recorded. Only the part of the kite boundary that is well illuminated by the array can be observed in the imaging function.

V. CONCLUSIONS

We propose a direct imaging algorithm, the multi-tone method. The algorithm is simple and efficient because no forward solver or iteration is needed. This method provides a framework for balancing spatial diversity via the singular value decomposition with frequency diversity via superposition of coherent phases. By taking advantage of phase coherence of multiple frequencies, the imaging is enhanced and is robust with respect to noise. The algorithm can deal with limited or synthetic aperture data naturally as well as with different material properties and different types of illuminations and measurements. More rigorous analysis will be carried out in our future study.

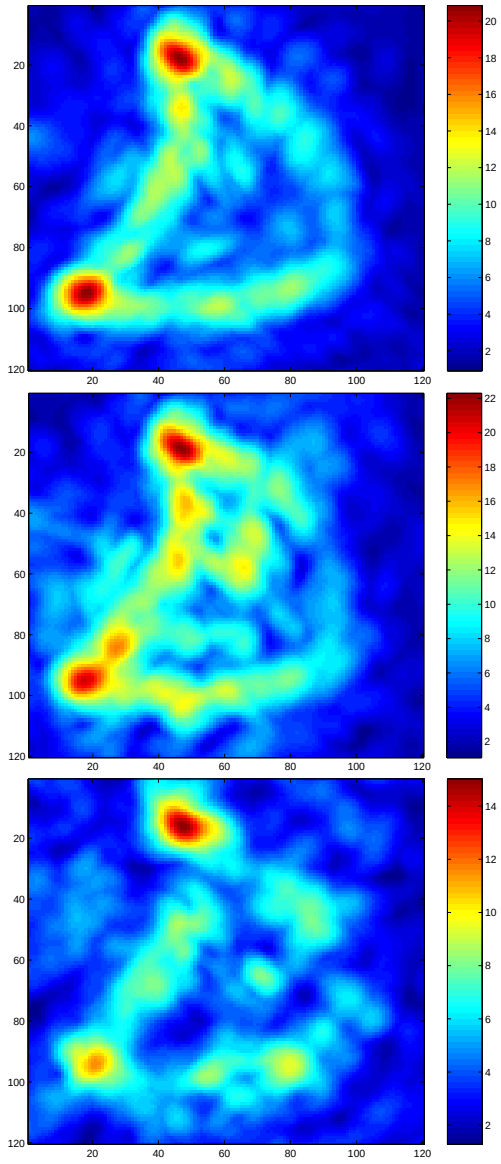

FIG. 10. Synthetic aperture multi-tone imaging for a kite shape with clean data on the top, 10% multiplicative noise in the middle and 10% random medium fluctuations on the bottom

Acknowledgments

We would like to thank our our collaborators at Carnegie Mellon University, J. M. F. Moura, D. Stancil, and J. Zhu for providing us the experimental data.

The research is partially supported by ONR grant N00014-02-1-0090, DARPA grant N00014-02-1-0603, NSF grant 0307011 the Sloan Foundation, and Louisiana Board of Re-

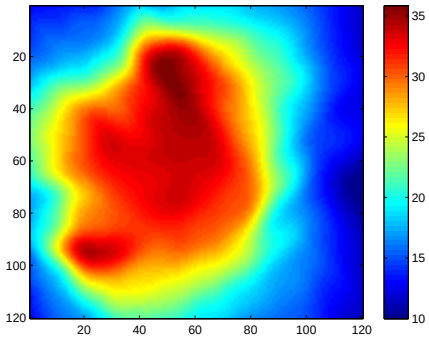

FIG. 11. MUSIC imaging function for a kite shape with clean synthetic aperture data. The result is poor.

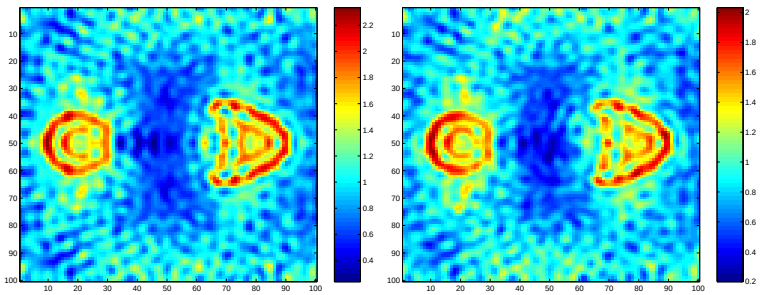

FIG. 12. Multi-tone imaging for a kite shape and a circular shape using far field data with 100% multiplicative noise.

gents RCS grant LEQSF(2008-11)-RD-A-18.

References

[1] Devaney, "Super-resolution processing of multi-static data using time-reversal and MUSIC", to appear in Journal of the Acoustical Society of America .

[2] A. J. D. F. K. Gruber, E. A. Marengo, "Time-reversal imaging with multiple signal classification considering multiple scattering between the targets", (2004).

[3] F. K. Gruber, E. A. Marengo, and A. J. Devaney, "Time-reversal imaging with multiple signal classification considering multiple scattering between the targets", J. Acoust. Soc. Am. **115**, 3042–3047 (2004).

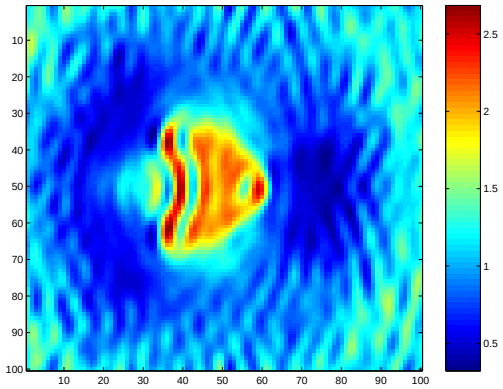

FIG. 13. Multi-tone imaging for a kite shape with incident plane wave directions different from recorded far field data directions

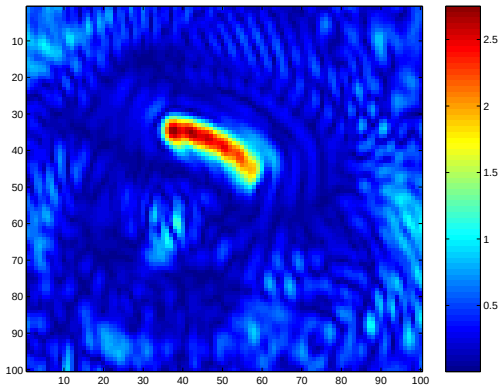

FIG. 14. Multi-tone imaging with limited aperture far-field data

[4] E. Kerbrat, C. Prada, and M. Fink, "Imaging in the presence of grain noise using the decomposition of the time reversal operator", Journal of the Acoustical Society of America **113(3)**, 1230–1240 (2003).

[5] C. Prada and J.-L. Thomas, "Experimental subwavelength localization of scatterers by decomposition of the time reversal operator interpreted as a covariance matrix", Journal of the Acoustical Society of America **114(1)**, 235–243 (2003).

[6] R. O. Schmidt, "Multiple emitter location and signal parameter estimation", IEEE Trans. Antennas Propagation. **34**, 276–280 (1986).

[7] E. Kerbrat, C. Prada, D. Cassereau, and M. Fink, "Ultrasonic nondestructive testing of scattering media using the decomposition of the time reversal operator", IEEE Trans.

Ultrason., Ferroelec., Freq. Contr. **49(8)**, 1103–1113 (2002).

[8] J.-G. Minonzio, C. Prada, D. Chambers, D. Clorennec, and M. Fink, "Characterization of subwavelength elastic cylinders with the decomposition of the time-reversal operator: Theory and experiment", J. Acoust. Soc. Am. **117**, 789–798 (2005).

[9] G. Montaldo, M. Tanter, and M. Fink, "Real time inverse filter focusing by iterative time reversal", J. Acoust. Soc. Am. **115**, 768–775 (2004).

[10] G. Montaldo, M. Tanter, and M. Fink, "Revisiting iterative time reversal processing: Application to detection of multiple targets", J. Acoust. Soc. Am. **115**, 776–784 (2004).

[11] C. Prada, S. Manneville, D. Spoliansky, and M. Fink, "Decomposition of the time reversal operator: Detection and selective focusing on two scatterers", Journal of the Acoustical Society of America **99**, 2067–2076 (1996).

[12] C. Prada, J.-L. Thomas, and M. Fink, "The iterative time reversal process: Analysis of the convergence", Journal of the Acoustical Society of America **97**, 62–71 (1995).

[13] S. Hou, K. Solna, and H. Zhao, "A direct imaging algorithm for extended targets", Inverse Problems **22**, 1151–1178 (2006).

[14] S. Hou, K. Solna, and H. Zhao, "A direct imaging method using far field data", Inverse Problems **23**, 1533–1546 (2007).

[15] E. Marengo, F. Gruber, and F. Simonetti, "Time-reversal music imaging of extended targets", IEEE Transactions on Image Processing (2007).

[16] E. Marengo, R. Hernandez, and H. Lev-Ari, "Intensity-only signal-subspace-based imaging", Journal of the Optical Society of America A (2007).

[17] *Theoretical Acoustics* (Princeton University Press) (1968).

[18] D. Chambers and A. Gautesen, "Time reversal for a single spherical scatter", Journal of the Acoustical Society of America **109**, 2616–2614 (2001).

[19] D. H. Chambers, J. V. Candy, S. K. Lehman, J. S. Kallman, A. J. Poggio, and A. W. Meyer, "Time reversal and the spatio-temporal matched filter (l)", J. Acoust. Soc. Am. **116**, 1348–1350 (2004).

[20] M. Tanter, J.-F. Aubry, J. Gerber, J.-L. Thomas, and M. Fink, "Optimal focusing by

spatio-temporal inverse filter. i. basic principles", J. Acoust. Soc. Am. **110**, 37–47 (2001).

[21] M. Tanter, J.-L. Thomas, and M. Fink, "Time reversal and the inverse filter", J. Acoust. Soc. Am. **108**, 223–234 (2000).

[22] L. Borcea, G. Papanicolaou, and C. Tsogka, "Coherent interferometric imaging", Geophysics **71**, 5139–516S1165–S1175 (2006).

[23] D. H. Chambers and J. G. Berryman, "Analysis of the time-reversal operator for a small spherical scatterer in an electromagnetic field", IEEE Trans. Ant. Prop. **52(7)**, 1729–1738 (2004).

[24] D. H. Chambers and J. G. Berryman, "Time-reversal analysis for scatterer characterization", Phys. Rev. Letters **92(2)**, 023902–1–023902–4 (2004).

[25] D. H. Chambers, "Analysis of the time-reversal operator for scatterers of finite size", J. Acoust. Soc. Am. **111(5)**, 411–419 (2002).

[26] S. Hou, K. Solna, and H. Zhao, "Imaging of location and geometry for extended targets using the response matrix", Journal of Computational Physics **199 (1)**, 317–338 (2004).

[27] H. Zhao, "Analysis of the response matrix for an extended target", SIAM Applied Mathematics **64 (3)**, 725–745 (2004).

[28] J.-P. Berenger, "A perfectly matched layer for the absorption of electromagnetic waves", J. Computational Physics **114**, 185–200 (1994).

[29] D. Colton and R. Kress, "Inverse acoustic and electromagnetic scattering theory, 2nd edition", Springer, Berlin (1998).

List of Figures